

Daisuke Miyazaki, Noriyuki Takashima, Akira Yoshida, Eiki Harashima, Katsushi Ikeuchi,
"Polarization-based Shape Estimation of Transparent Objects by Using Raytracing and PLZT
Camera,"
in Proceedings of SPIE (Polarization Science and Remote Sensing II, Part of SPIE's International
Symposium on Optics and Photonics 2005),
Vol. 5888, pp. 1-14, San Diego, CA USA, Aug. 2005.

Polarization-based Shape Estimation of Transparent Objects by Using Raytracing and PLZT Camera

Daisuke Miyazaki^a, Noriyuki Takashima^b, Akira Yoshida^b, Eiki Harashima^b, and Katsushi Ikeuchi^a

^aThe University of Tokyo, 4-6-1 Komaba, Meguro-ku, Tokyo, 153-8505 JAPAN;

^bFuruuchi Chemical Corporation, 6-17-17 Minamioi, Shinagawa-ku, Tokyo, 140-0013 JAPAN

ABSTRACT

In the first part of this paper, we present a method to estimate the shape of transparent objects by using polarization. Few existing methods for this procedure consider internal interreflection, which is a multiple reflection occurring inside the transparent object. Our proposed method considers such interreflection by using the raytracing method. Also, we calculate the polarization state of the light using Mueller calculus. We then combine these methods to produce rendered polarization data. The shape of the object is computed by an iterative framework that minimizes the difference between the obtained polarization data and the rendered polarization data. In the second part of this paper, we present an apparatus to measure the polarization state of the light. To analyze the light, we use a material called PLZT whose material state changes with the applied voltage. We obtain the polarization state of the light by controlling the voltage of the PLZT from the computer. In the last part of this paper, we present some experimental results using the proposed method and apparatus.

Keywords: Mueller calculus, PLZT, Transparent object, Shape-from-X, Raytracing

1. INTRODUCTION

In the field of computer vision, few methods have been proposed for estimating the shape of transparent objects, because of the difficulty of dealing with mutual reflection, which is the phenomenon that the light not only reflects at the surface of the transparent object but also transmits into the object and causes multiple reflections and transmissions inside it. We use the term “interreflection” for such internal reflection. For the first part of this paper,¹ we present a method for estimating the surface shape of transparent objects by using the raytracing method and Mueller calculus. For the second part of this paper, we present a device for measuring the Stokes parameters of the observed light by using PLZT.

Much research has been done on the polarization phenomenon.² By analyzing the polarization phenomenon, Schechner et al.³ decomposed the reflected scene and the transmitted scene that were originally combined with a glass plate. Wolff and Boulton,⁴ Nayar et al.,⁵ Lin and Lee,⁶ and Umeyama and Godin⁷ separated the specular reflection component and the diffuse reflection component of the image by polarization analysis. In the field of computer graphics, a polarizing filter is also used to separate the specular reflection component from the diffuse reflection component to estimate the parameters of BRDF (Bidirectional Reflectance Distribution Function).⁸⁻¹¹ Schechner et al.^{12,13} used polarization to improve the quality of images taken in hazy weather and under water. Schechner et al.¹⁴ also developed a device and an algorithm to obtain polarization data in a wide field of view. By using a polarizer, Cula et al.¹⁵ decomposed the image taken under multiple light sources into the images taken under each light sources. Clark et al.¹⁶ and Wallace et al.¹⁷ improved the laser range finder by polarization analysis to estimate the shape of opaque objects. Wolff, Boulton, and Chen^{4,18,19} used polarization analysis to classify material into metal or dielectric. Sandus,²⁰ Nicodemus,^{21,22} Jordan et al.^{23,24} and Wolff et al.²⁵ analyzed the degree of polarization in infrared wavelengths. There are roughly four kinds of methods to calculate the polarization state of the light: (1) a simple calculation method using Fresnel formulae,^{2,26,27} (2) a method using a coherence matrix,²⁶ (3) Mueller calculus,^{2,27} and (4) Jones calculus.^{2,27} Some commercial raytracing software²⁸⁻³⁰ simulates the polarization state by using these methods. Kagalwala and Kanade³¹ used Jones calculus to simulate the structure of the Nomarski DIC (Differential Interference Contrast) microscope. Koshikawa and Shirai³² used Mueller calculus to estimate the surface normal of specular polyhedrons. Gondek et al.³⁶ calculated the polarization state of the light by using the raytracing method and Fresnel formulae. Wolff and Kurlander³³ calculated the polarization state of the light

Further author information: (Send correspondence to Daisuke Miyazaki.)

Daisuke Miyazaki: E-mail: miyazaki@cvl.iis.u-tokyo.ac.jp, Telephone: +81 (0)3 5452 6242

by using the raytracing method and a coherence matrix. Later, Tannenbaum et al.³⁷ and Guy and Soler³⁹ extended this method. Gu and Yeh³⁵ extended the Jones calculus method. Chipman³⁴ also extended the Jones calculus method, which can be easily combined with the raytracing method. Wilkie et al.³⁸ calculated the polarization state of the light by using the raytracing method and Mueller calculus. Wolff et al.,⁴⁰ Fujikake et al.,⁴¹ and Harnett and Craighead⁴² developed a polarization camera with liquid crystal, which is controllable from a computer. A material called PLZT has a polarization characteristic and is used in many application fields.⁴³ The polarization characteristic of PLZT is analyzed by Shames et al.⁴⁴

Recently, research to estimate the shape of the object by using polarization has increased. Koshikawa and Shirai³² proposed to use the degree of polarization, employing circularly polarized light sources to determine the surface normal of specular polyhedrons. They used Mueller calculus to calculate the polarization state of the light. Wolff and Boulton⁴ indicated that the surface normal of the object surface is constrained by analyzing the polarization of the object, and estimated the surface normal of a planar glass from two views. Rahmann⁴⁵ estimated the orientation of a flat object and the position of the light source by polarization analysis of a single view. Rahmann also⁴⁶ addressed the potential of recovering the shape of specular surfaces from polarization. Later, Rahmann and Canterakis⁴⁷ estimated the shape of specular objects from two or more views. Also, they proved that the quadratic shape of specular objects can be estimated from two views.⁴⁸ Drbohlav and Šára⁴⁹ estimated the shape of diffuse objects by combining polarization analysis and photometric stereo. Miyazaki et al.⁵⁰ estimated the shape and reflectance of specular objects and the illuminant direction from one view. Saito et al.⁵¹ and Miyazaki et al.^{52, 53} estimated the surface shape of transparent objects by means of polarization analysis. Unfortunately, because these methods do not consider interreflection, they do not provide sufficient accuracy for estimating the shape of transparent objects.

Many methods have been developed to deal with transparent objects. Recently, a method called environment mapping⁵⁴⁻⁵⁹ has been developed for graphics applications that render transparent objects. When one watches at a planar glass such as a window, one can see both the reflection of the foreground scene and the transmission of the background scene. Farid and Adelson,⁶⁰ Schechner et al.,^{3, 61} Szeliski et al.,⁶² and Levin et al.⁶³ attempted to separate the two scenes by observing the composite image of the two scenes. Nikolaev and Nayar⁶⁴ developed a transparent robot arm, which helps the robot to recognize what it is grasping. Osadchy et al.⁶⁵ used the specularity of transparent objects for object recognition. From the image of natural scene, McHenry et al.⁶⁶ detected the edge of transparent objects by using the fact that the color of the pixels between one side of the edge and the other side of the edge is similar. These methods, however, do not provide total information about the shape of the transparent object.

Some methods that estimate the 3D shape of transparent objects have been proposed. Murase⁶⁷ estimated the shape of a water surface by analyzing the undulation of that surface. Hata et al.⁶⁸ estimated the surface shape of transparent objects by analyzing the deformation of the light projected onto the transparent objects. Ohara et al.⁶⁹ estimated the depth of the edge of a transparent object by using shape-from-focus. Ben-Ezra and Nayar⁷⁰ estimated the parameterized surface shape of transparent objects by using structure-from-motion. Kutulakos⁷¹ estimated both the depth and the surface normal of transparent objects by multiple viewpoints and multiple light sources. Saito et al.⁵¹ and Miyazaki et al.^{52, 53} estimated the surface shape of transparent objects by means of polarization analysis. None of these methods are capable of estimating arbitrary shapes of transparent objects.

For the first part of this paper, we simulate the interreflection of transparent objects by using the raytracing method and Mueller calculus, and we use this method to estimate the surface shapes of transparent objects that have arbitrary shapes. For the second part of this paper, we simulate the state of the material called PLZT by Mueller calculus, and we use this material to measure the polarization state of the observed light.

The rest of the paper is organized as follows. In Section 2, we explain the method that estimates the surface shapes of transparent objects by using the raytracing method and Mueller calculus. In Section 3, we explain the method that measures the polarization state of the light by using PLZT and Mueller calculus. Our measurement results are shown in Section 4, and our conclusions are presented in Section 5.

2. TRANSPARENT SURFACE MODELING

The theoretical details of the principle of polarization, which appears in this section, are presented in the literature.^{2, 26, 27}

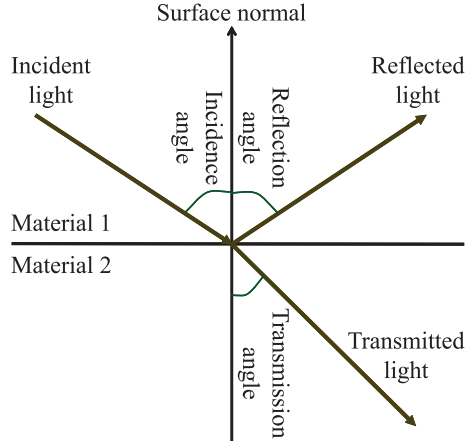


Figure 1. Reflection, refraction, and transmission.

2.1. Polarization Raytracing

Figure 1 describes the light reflected and transmitted between material 1 and material 2. We assume that the surface of transparent objects is optically smooth; thus, the incidence angle is equal to the reflection angle. The transmission angle is related to the incidence angle as the following Snell's law:

$$\sin \theta = n \sin \theta' \quad , \quad (1)$$

where θ is the incidence angle, θ' is the transmission angle, and n is the ratio of the refractive index of material 2 to that of material 1. In this paper, we assume that the refractive index of one object is a scalar value which is, at the same time, constant throughout any part of the object. Therefore, this paper does not focus on birefringent materials. The plane of incidence (POI) is a plane that includes the surface normal direction, the incident light direction, the reflected light direction, and the transmitted light direction.

Subscripts \parallel and \perp represent the components parallel and perpendicular to the POI, respectively. Parallel and perpendicular components of intensity reflectivity are represented as R_{\parallel} and R_{\perp} , respectively, while those of intensity transmissivity are represented as T_{\parallel} and T_{\perp} , respectively. These values are defined as follows:

$$R_{\parallel} = \frac{\tan^2(\theta - \theta')}{\tan^2(\theta + \theta')} \quad , \quad R_{\perp} = \frac{\sin^2(\theta - \theta')}{\sin^2(\theta + \theta')} \quad , \quad T_{\parallel} = \frac{\sin 2\theta \sin 2\theta'}{\sin^2(\theta + \theta') \cos^2(\theta - \theta')} \quad , \quad T_{\perp} = \frac{\sin 2\theta \sin 2\theta'}{\sin^2(\theta + \theta')} \quad . \quad (2)$$

Brewster angle θ_B is defined as follows:

$$\tan \theta_B = n \quad . \quad (3)$$

Critical angle θ_C is defined as follows:

$$\sin \theta_c = n \quad . \quad (4)$$

For the total reflection, we must use $R_{\parallel} = R_{\perp} = 1$ and $T_{\parallel} = T_{\perp} = 0$.

In this paper, we call the raytracing method that considers the polarization effect the polarization raytracing method. The algorithm of the polarization raytracing method can be divided into two parts. For the first part, the calculation of the propagation of the ray, we employ the same algorithm used in the conventional raytracing method. For the second part, the calculation of the polarization state of the light, we employ Mueller calculus in this paper because of its simplicity of description, along with its ease of understanding and implementation. These three methods have almost identical functions; thus, all discussions presented in this paper are also applicable to other calculi. Stokes vector $\mathbf{s} = (s_0, s_1, s_2, s_3)^T$, a 4D vector, represents the polarization state of the light, and the Mueller matrix \mathbf{M} , a 4×4 matrix, represents how the object changes the polarization state of the light.

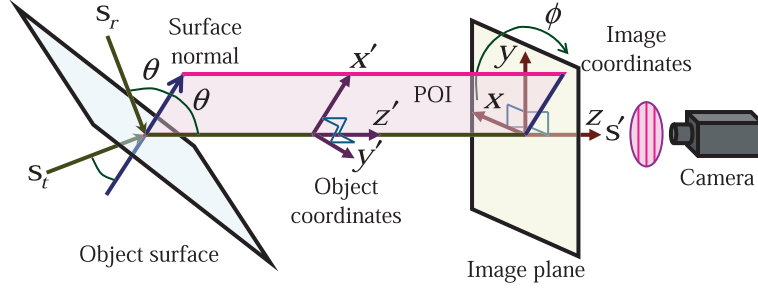


Figure 2. Reflected and transmitted light observed by the camera.

Here we present an example of calculation. Suppose the geometrical setup when the reflected and transmitted light is observed from the camera is as described in Figure 2. In this figure, there are two kinds of coordinates systems: $x'y'z'$ coordinates and xyz coordinates. Here, the z' axis and the z axis are the same. x' is included in the POI and is facing to the same side as the surface normal is facing. The angle between x' axis and x axis is called the POI angle ϕ in xyz coordinates.

In the case presented in Figure 2, observed light is a composition of reflected light and transmitted light. The Stokes vector s' of the observed light is calculated as follows:

$$s' = C(\phi)D(\delta; n)R(\theta; n)C(-\phi)s_r + C(\phi)T(\theta; n)C(-\phi)s_t \quad (5)$$

Stokes vectors of the incident light are represented as s_r and s_t , where s_r and s_t represent the lights that are set in the origin of the reflection and transmission, respectively. C is the rotation Mueller matrix and is given by:

$$C(\phi) = \begin{pmatrix} 1 & 0 & 0 & 0 \\ 0 & \cos 2\phi & -\sin 2\phi & 0 \\ 0 & \sin 2\phi & \cos 2\phi & 0 \\ 0 & 0 & 0 & 1 \end{pmatrix} \quad (6)$$

R and T are the reflection Mueller matrix and the transmission Mueller matrix, respectively, which are represented as follows:

$$R = \begin{pmatrix} (R_{\parallel} + R_{\perp})/2 & (R_{\parallel} - R_{\perp})/2 & 0 & 0 \\ (R_{\parallel} - R_{\perp})/2 & (R_{\parallel} + R_{\perp})/2 & 0 & 0 \\ 0 & 0 & \sqrt{R_{\parallel}R_{\perp}} & 0 \\ 0 & 0 & 0 & \sqrt{R_{\parallel}R_{\perp}} \end{pmatrix}, \quad T = \begin{pmatrix} (T_{\parallel} + T_{\perp})/2 & (T_{\parallel} - T_{\perp})/2 & 0 & 0 \\ (T_{\parallel} - T_{\perp})/2 & (T_{\parallel} + T_{\perp})/2 & 0 & 0 \\ 0 & 0 & \sqrt{T_{\parallel}T_{\perp}} & 0 \\ 0 & 0 & 0 & \sqrt{T_{\parallel}T_{\perp}} \end{pmatrix} \quad (7)$$

However, if the total reflection occurs, then R and T are set to be identity matrix and zero matrix, respectively. D is the retardation Mueller matrix and is given as:

$$D(\delta) = \begin{pmatrix} 1 & 0 & 0 & 0 \\ 0 & 1 & 0 & 0 \\ 0 & 0 & \cos \delta & \sin \delta \\ 0 & 0 & -\sin \delta & \cos \delta \end{pmatrix}, \quad (8)$$

where δ is the amount of the phase shift (or retardation). The phase of the reflected light shifts when the total reflection occurs. Also, the phase of the reflected light inverts when the incidence angle is smaller than the Brewster angle θ_B . Consequently, the value of δ is set as follows:

$$\delta = \begin{cases} \text{Eq.(10)} & \theta \geq \theta_C \\ 180^\circ & \theta \leq \theta_B \\ 0^\circ & \text{otherwise} \end{cases}, \quad (9)$$

$$\tan \frac{\delta}{2} = \frac{\cos \theta \sqrt{\sin^2 \theta - n^2}}{\sin^2 \theta} \quad (10)$$

2.2. Inverse Polarization Raytracing

In this section, we introduce our method for estimating the front surface shape of a transparent object using the Stokes vector as an input under the assumption that the refractive index, the shape of the back surface, and the illumination distribution are given. Details of numerical algorithms are presented in the literature.^{7,2}

We denote the input polarization data as I_E . Polarization data are represented as an image (2-dimensionally distributed data) where the Stokes vector is set for each pixel. The polarization raytracing explained in Section 2.1 can render the polarization data from the shape of the transparent object by tracing the light ray and by Mueller calculus. We denote this rendered polarization image as I_R . The shape of transparent objects is represented as the height H , set for each pixel. Heights partially differentiated by x and y are called gradients, and are represented as p and q , respectively:

$$p = H_x = \frac{\partial H}{\partial x}, \quad q = H_y = \frac{\partial H}{\partial y}. \quad (11)$$

Surface normal $\mathbf{n} = (-p, -q, 1)^T$ is represented by these gradients.

The rendered polarization image I_R depends upon height and surface normal, so it can be represented as $I_R(H, p, q)$. A straightforward definition of the cost function, which we want to minimize, can be as follows:

$$\iint E_1(x, y) dx dy, \quad \text{where } E_1 = (I_E - I_R(H, p, q))^2. \quad (12)$$

We will sometimes omit the variables (x, y) in the subsequent discussions for simplicity of description. I_R depends upon p , q , and H , while p , q , and H depend upon each other per Equation (11). Thus, the cost function must be modified as follows:

$$\iint (\lambda E_1 + E_2) dx dy, \quad \text{where } E_2 = (H_x - p)^2 + (H_y - q)^2. \quad (13)$$

λ is a Lagrange undetermined multiplier.

Euler equations that minimize Equation (13) are derived as follows:

$$p = H_x - \frac{\lambda}{2} \frac{\partial E_1}{\partial p}, \quad q = H_y - \frac{\lambda}{2} \frac{\partial E_1}{\partial q}, \quad H = \bar{H} - \frac{1}{4} (p_x + q_y) - \frac{\lambda}{8} \frac{\partial E_1}{\partial H}, \quad (14)$$

where \bar{H} is a 4-neighbor average of H .

Each of the above equations can be decomposed into two steps:

$$p^{(k)} = H_x^{(k)}, \quad (15) \quad p^{(k+1)} = p^{(k)} - \lambda_1^{(k+1)} \frac{\partial E_1^{(k)}}{\partial p}, \quad (16)$$

$$q^{(k)} = H_y^{(k)}, \quad (17) \quad q^{(k+1)} = q^{(k)} - \lambda_2^{(k+1)} \frac{\partial E_1^{(k)}}{\partial q}, \quad (18)$$

$$H^{(k+1)} = \bar{H}^{(k)} - \frac{1}{4} (p_x^{(k+1)} + q_y^{(k+1)}) \quad (19) \quad H^{(l)} = H^{(l)} - \lambda_3^{(l)} \frac{\partial E_1^{(l)}}{\partial H}. \quad (20)$$

Here, λ_1 , λ_2 , and λ_3 are scalar values that are determined for each pixel and for each iteration step. Superscript (k) represents the iteration number. We do not write down the iteration number for Equation (20) because we do not use this equation. One reason is that the cost function E_1 depends upon the change of surface normal rather than on the change of height. Another reason is that the cost function E_1 smoothly changes when the surface normal changes, but it does not smoothly change when the height changes. This fact was empirically proved in the preliminary experiments.

The algorithm goes as follows. First, we set initial values of shape H for each point of the front surface. Next, p and q are calculated by Equations (15)(17). Then, we solve Equations (16)(18). λ_1 and λ_2 should be optimal values; thus, we use Brent's method to determine λ_1 and λ_2 , which minimizes the cost function E_1 . After computing p and q at every pixel, we solve Equation (19) by the relaxation method^{7,3,7,4} to determine the height H . We use the alternating-direction implicit method to solve the relaxation problem. To conclude, the front surface shape of the transparent object is estimated by an iterative computation, where each step of iteration solves Equations (15)–(19), and the iteration stops when Equation (12) is minimized.

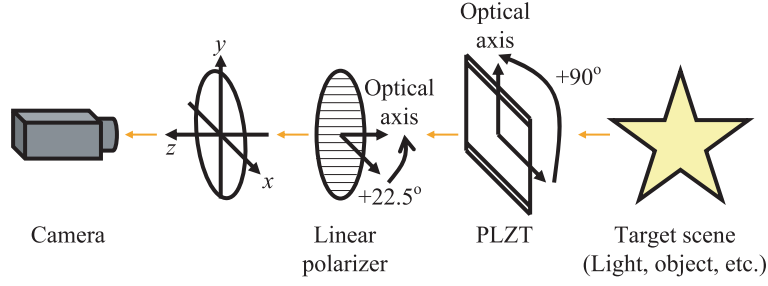


Figure 3. System of PLZT and linear polarizer.

3. PLZT POLARIZATION CAMERA

3.1. PLZT

PLZT^{43, 44} (lanthanum modified lead zirconate-lead titanate), $(\text{Pb}, \text{La})(\text{Zr}, \text{Ti})\text{O}_3$, consists of a set of compositions and is a transparent ferroelectric ceramic material. The procedure to fabricate the PLZT is roughly as follows: first, mix tetrabutyl zirconate, tetrabutyl titanate, lead oxide, and lanthanum acetate; next, dry the precipitate; and finally, PLZT is obtained by hot pressing the dried precipitate. PLZT is a birefringence medium, and it acts like a retarder (or waveplate). The optical properties of PLZT depends on the electric field. By changing the amount of electric field, PLZT will act like a half-wave plate, a quarter-wave plate, etc. Please refer to Shames et al.⁴⁴ for the polarization characteristic of PLZT.

Some researchers⁴⁰⁻⁴² developed polarization cameras with liquid crystal, which is controllable from a computer. However, they only measure the first three components of the Stokes vector. We developed a polarization camera with PLZT, which is controllable from a computer, and which can measure all four components of the Stokes vector.

3.2. PLZT and Linear Polarizer

In this section, we explain about the setup described in Figure 3. We set the $+z$ -axis heading toward the camera. Then we set the linear polarizer in front of the camera, whose optical axis is rotated $+22.5^\circ$ from $+x$ -axis to $+y$ -axis. Finally, we set the PLZT in front of the linear polarizer, whose optical axis is the same as the y -axis.

The Mueller matrix of the horizontal linear polarizer, whose optical axis is the same as the x -axis, is represented as follows:

$$\mathbf{L} = \frac{1}{2}F_A \begin{pmatrix} 1 & 1 & 0 & 0 \\ 1 & 1 & 0 & 0 \\ 0 & 0 & 0 & 0 \\ 0 & 0 & 0 & 0 \end{pmatrix}, \quad (21)$$

where $F_A \leq 1$, and $F_A = 1$ for an ideal linear polarizer. The value of F_A for the actual linear polarizer is obtained in the preliminary experiments. The Mueller matrix of rotation is represented in Equation (6). Thus, the Mueller matrix $\hat{\mathbf{L}}$ of the linear polarizer whose optical axis rotated as $+22.5^\circ$ will be:

$$\hat{\mathbf{L}} = \mathbf{C}(+22.5^\circ)\mathbf{L}\mathbf{C}(-22.5^\circ) \quad (22)$$

PLZT acts like a retarder depending on the voltage pressing to the PLZT. The Mueller matrix of retardation is represented in Equation (8). Thus, the Mueller matrix $\hat{\mathbf{D}}(\delta)$ of the PLZT whose optical axis is the same as y -axis will be:

$$\hat{\mathbf{D}}(\delta) = \mathbf{C}(+90^\circ)\mathbf{D}(\delta)\mathbf{C}(-90^\circ) \quad (23)$$

As a result, the Mueller matrix $\mathbf{M}_{\text{PL}}(\delta)$ of the system illustrated in Figure 3 will be:

$$\mathbf{M}_{\text{PL}}(\delta) = \hat{\mathbf{L}}\hat{\mathbf{D}}(\delta) \quad (24)$$

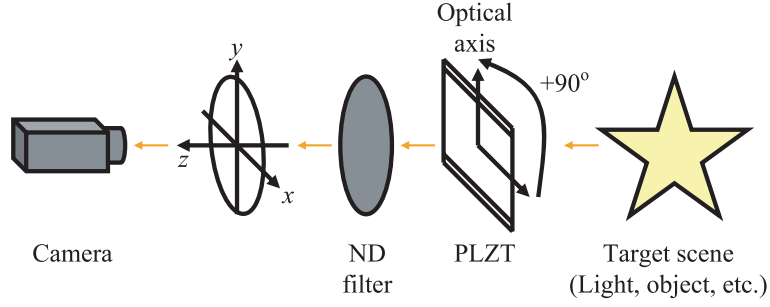


Figure 4. System of PLZT and ND filter.

PLZT has a hysteresis and acts as a retarder even if there is no electric current streaming inside the PLZT. The Mueller matrix in this case will be $M_{PL}(\delta)$, where δ is determined in the preliminary experiments. PLZT acts like a quarter-wave plate when the voltage of the PLZT is increased in a certain value. The amount of the voltage is determined in the preliminary experiments. In this case, $\delta = \pi/2$, thus, the Mueller matrix will be $M_{PL}(\pi/2)$. PLZT acts like a half-wave plate when the voltage of the PLZT is increased in a certain value. The amount of the voltage is determined in the preliminary experiments. In this case, $\delta = \pi$. Thus, the Mueller matrix will be $M_{PL}(\pi)$.

3.3. PLZT and ND Filter

In this section, we explain about the setup described in Figure 4. We set the $+z$ -axis heading toward the camera. Then we set the ND (neutral density) filter in front of the camera. Finally, we set the PLZT in front of the ND filter, whose optical axis is the same as the y -axis.

The Mueller matrix of ND filter is represented as follows:

$$\mathbf{N} = F_B \begin{pmatrix} 1 & 0 & 0 & 0 \\ 0 & 1 & 0 & 0 \\ 0 & 0 & 1 & 0 \\ 0 & 0 & 0 & 1 \end{pmatrix}, \quad (25)$$

where $F_B \leq 1$. The value of F_B for the actual ND filter is obtained a priori.

As a result, the Mueller matrix $M_{ND}(\delta)$ of the system illustrated in Figure 4 will be:

$$\mathbf{M}_{ND}(\delta) = \mathbf{N} \hat{\mathbf{D}}(\delta) \quad (26)$$

3.4. Stokes Vector

The light that has a Stokes vector $(s_{0i}, s_{1i}, s_{2i}, s_{3i})^T$, first transmits through the PLZT and the linear polarizer or the ND filter, and then is observed by the camera. Only the first component of Stokes vector is observed by the camera because it represents the intensity of the light. We denote the intensity observed by the system suggested in Section 3.2 when there is no voltage in the PLZT as $s_{0,PL,0}$. The intensity is calculated by the Mueller matrix $M_{PL}(\delta)$. Next, we denote the intensity observed by the system suggested in Section 3.2 when the PLZT acts like a quarter-wave plate as $s_{0,PL,\lambda/4}$. The intensity is calculated by the Mueller matrix $M_{PL}(\pi/2)$. We also denote the intensity observed by the system suggested in Section 3.2 when the PLZT acts like a half-wave plate as $s_{0,PL,\lambda/2}$. The intensity is calculated by the Mueller matrix $M_{PL}(\pi)$. Finally, we denote the intensity observed by the system suggested in Section 3.3 as $s_{0,ND}$. The intensity is calculated by the Mueller matrix $M_{ND}(\delta)$.

By concatenating the four equations, which are related to $s_{0,PL,0}$, $s_{0,PL,\lambda/4}$, $s_{0,PL,\lambda/2}$, and $s_{0,ND}$, these equations can be expressed in a matrix as follows:

$$\begin{pmatrix} s_{0,PL,0} \\ s_{0,PL,\lambda/4} \\ s_{0,PL,\lambda/2} \\ s_{0,ND} \end{pmatrix} = \begin{pmatrix} \frac{1}{2}F_A & \frac{\sqrt{2}}{4}F_A & \frac{\sqrt{2}}{4}\cos\delta F_A & -\frac{\sqrt{2}}{4}\sin\delta F_A \\ \frac{1}{2}F_A & \frac{\sqrt{2}}{4}F_A & 0 & -\frac{\sqrt{2}}{4}F_A \\ \frac{1}{2}F_A & \frac{\sqrt{2}}{4}F_A & -\frac{\sqrt{2}}{4}F_A & 0 \\ F_B & 0 & 0 & 0 \end{pmatrix} \begin{pmatrix} s_{0i} \\ s_{1i} \\ s_{2i} \\ s_{3i} \end{pmatrix} \quad (27)$$

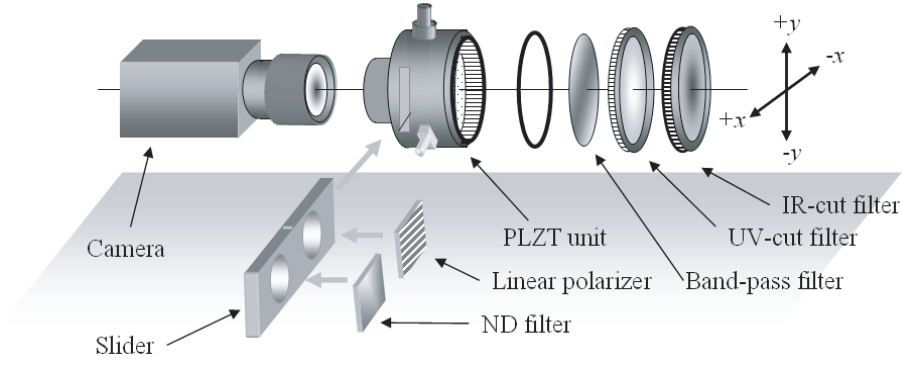


Figure 5. Acquisition System “Polavision”.

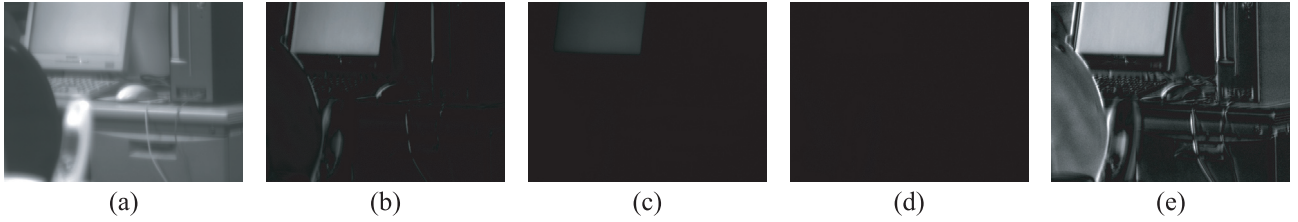


Figure 6. Measurement result of Polavision: (a) s_0 , (b) s_1 , (c) s_2 , (d) s_3 , and (e) DOP.

By calculating the inverse matrix in the above equation, we can calculate the Stokes vector $(s_{0i}, s_{1i}, s_{2i}, s_{3i})^T$ of the light of the target.

4. MEASUREMENT RESULT

4.1. Acquisition System “Polavision”

For obtaining the polarization state of the light by using PLZT, we developed an acquisition system that we named “Polavision” (Figure 5). First, the slider is set in front of the camera, which switches the linear polarizer and the ND filter. Next, PLZT is set in front of the slider. Finally, band-pass filters are set in front of the system to observe only the light whose wavelength is around 540nm, since the performance of PLZT and polarizer will become the maximum around such wavelength.

First, we set the linear polarizer in front of the camera, and we obtain three images by setting three different electric voltages to the PLZT. Next, we change the polarizer into the ND filter, and we obtain one image with no electric voltage to the PLZT. From these four images, we calculate the Stokes parameters of the light.

4.2. Measurement Results of Polavision

The measurement result of an indoor scene is shown in Figure 6. Figures 6 (a) (b) (c) and (d) represent the four Stokes parameters, respectively. The degree of polarization (DOP) of the scene is shown in Figure 6 (e). The DOP represents how much the light is polarized and is defined as follows:

$$\hat{\rho} = \frac{\sqrt{s_1^2 + s_2^2 + s_3^2}}{s_0} \quad (28)$$

The white pixel represents the high value and the black pixel represents the low value in Figure 6. Figure 6 (e) tells us that the DOP of the liquid crystal display has a higher value because the liquid crystal display is polarized.

We also measured the linear polarizer and the left circular polarizer by Polavision. The measured DOP of the linear polarizer was 0.72. The true value must be 1. The measured fourth parameter s_3 of Stokes vector of the left circular

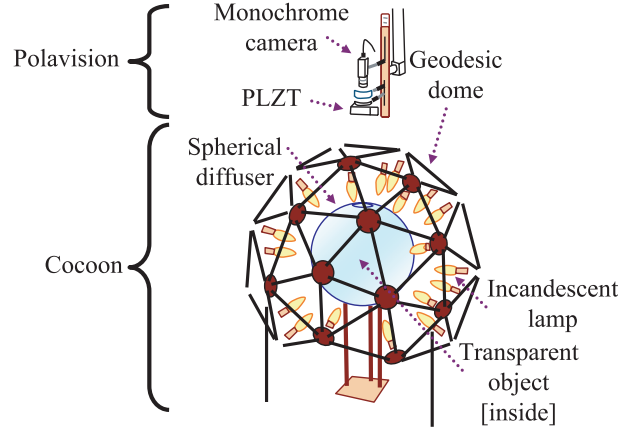


Figure 7. Acquisition System “Cocoon”.

polarizer was -0.25. The true value must be -1. These results indicate that the system can obtain the first three parameters of the Stokes vector in enough precision, while the system cannot precisely obtain the fourth parameter of the Stokes vector. Enhancing the precision of the fourth parameter of the Stokes vector will be our future work.

4.3. Acquisition System “Cocoon”

For obtaining polarization data to calculate the shape of transparent objects, we developed an acquisition system that we named “Cocoon” (Figure 7). The target object is set inside the center of a plastic sphere whose diameter is 35cm. This plastic sphere is illuminated by 36 incandescent lamps. These 36 light sources are almost uniformly distributed spatially around the plastic sphere by the geodesic dome. This geodesic dome, originally developed by Ikeuchi and Nayar,^{75–77} is a polyhedron generated by a 2nd order geodesation operation of an icosahedron. This dome has 42 vertices, 80 faces, and 120 edges; however, there are no triangles in the bottom part of the actual setup in order to support the geodesic dome. Later, Debevec et al.⁷⁸ developed a similar setup called “Light Stage” to sample the appearance of a human face under various illumination distributions. The plastic sphere diffuses the light that comes from the light sources, and it behaves as a spherical light source, which illuminates the target object from every direction. The target object is observed by monochrome camera from the top of the plastic sphere, which has a hole on the top. PLZT, linear polarizer, and ND filter are set in front of the camera. The Stokes vector is obtained by Polavision.

The DOP is defined in Equation (28). As shown in Section 4.2, the precision of the fourth parameter s_3 of the Stokes vector of Polavision is too low. Thus, for the shape estimation of transparent objects, we do not use the fourth parameter s_3 , and we calculate the DOP as follows:

$$\rho = \frac{\sqrt{s_1^2 + s_2^2}}{s_0} . \quad (29)$$

Now, we define phase angle ψ as follows:

$$\cos 2\psi = \frac{s_1}{\sqrt{s_1^2 + s_2^2}} , \quad \sin 2\psi = \frac{s_2}{\sqrt{s_1^2 + s_2^2}} . \quad (30)$$

In this paper, we use the DOP and the phase angle as inputs instead of using the Stokes vector as an input.

4.4. Measurement Results of Cocoon

4.4.1. Hemisphere

For the first measurement result of Cocoon, we observe an acrylic transparent hemisphere from the spherical part. We assume that the refractive index and the back surface shape are known. We also assume that the illumination distribution is known. This paper only concentrates on proposing a method to estimate the shapes of transparent objects, and does not focus on obtaining the correct illumination distribution.

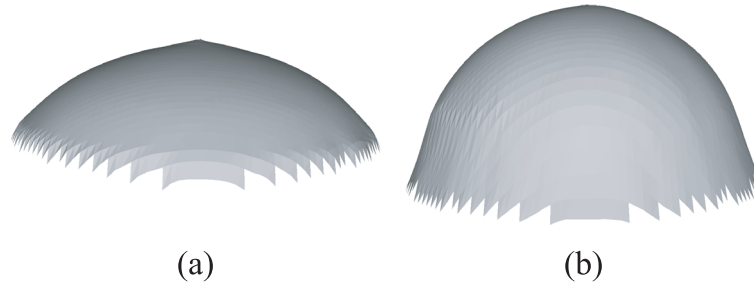


Figure 8. Estimation result of hemisphere: (a) Initial state (result of previous method), (b) result after 10 loops.

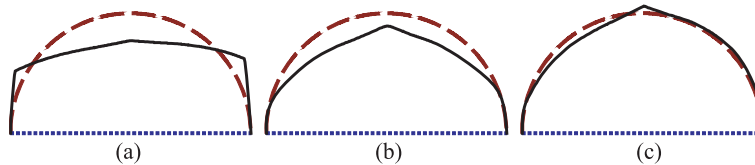


Figure 9. Estimation result: (a) Initial state (result of previous method), (b), (c) results after 5 and 50 loops.

The estimation result is shown in Figure 8. Figure 8 (a) represents the result of the previous method⁵¹⁻⁵³ and, at the same time, it represents the initial value. Figure 8 (b) is the result after 10 loops of our method.

More detailed evaluation is done in the 2D plane that is a cross-section of the 3D object, which includes the center of the base circle and the line perpendicular to that circle. The proposed algorithm estimates the front surface shape, a semicircle, by using the polarization data of the 2D plane as input data. The result of applying the proposed method is given in Figure 9 (c). In Figure 9, the solid line represents the estimated shape, and the dotted line represents the true shape. The result of the previous method (Figure 9 (a)) is used for the initial state of the shape. Figure 9 (b) and Figure 9 (c) are the results after 5 and 50 loops, respectively.

The RMS (Root Mean Square) error between the estimated value and the true value is used to compare the accuracy between the proposed method and the previous method. The RMS error of the surface normal was 23.3° for the previous method and 9.09° for our method. The RMS error of the height was 2.70 mm for the previous method and 0.672 mm for our method.

4.4.2. Bell-shaped Object

Now we observe the transparent object shown in Figure 10 (a). This object is made of acrylic and is a body-of-revolution. Its refractive index is 1.5 and its diameter at the base is 24 mm. The object is observed from the projected area. The front surface is a curved surface and the back surface is a disk. The camera is set orthogonally to the disk. We assume that the refractive index and the back surface shape are known. We also assume that the illumination distribution is known.

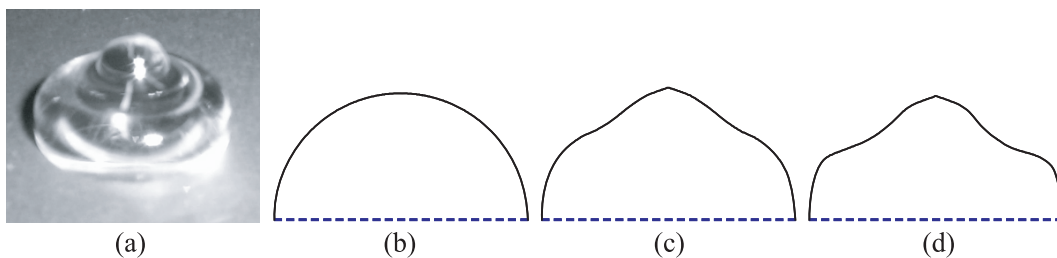


Figure 10. (a) Bell-shaped transparent acrylic real object. Estimation result: (b) Initial value, (c), (d) result after 5,20 loops.

We estimate the shape of a cross-section of the object to analyze the precision of the proposed method. The cross-section includes the center of the base circle and the line perpendicular to that circle. Figure 10 (d) illustrates the estimated shape of the object. The solid curve represents the obtained front height, and the dotted line represents the given back height. The initial value is set to be a semicircle shown in Figure 10 (b). The estimated shape after 5 and 20 loops is illustrated in Figure 10 (c) and Figure 10 (d), respectively. RMS of the height was 0.24 mm, where the true shape was obtained from the silhouette extracted manually by a human operator from the photograph of the object taken from the side.

5. CONCLUSION

In the first half of this paper, we proposed a novel method for estimating the surface shape of transparent objects by minimizing the difference between the input polarization data taken by observing the transparent object and the computed polarization data rendered by the polarization raytracing method. Experimental results showed that the accuracy of the method was higher than the previous method.^{51–53} We assumed that the back surface shape, the refractive index, and the illumination distribution are known. Relaxing such assumption will be our future work.

In the second half of the paper, we proposed a novel device for measuring the polarization state of the light by using a material called PLZT. We estimated the entire four parameters of the Stokes vector compared to other existing methods,^{40–42} which measure only the first three parameters of the Stokes vector. PLZT has a faster response than liquid crystal; thus, there is a potential that we can develop a faster measurement system than other methods that use liquid crystal. This measurement system is controllable from the computer, and can measure the polarization state of the light semi-automatically. However, this system requires a human operation for switching the filter during the measurement. Developing a real-time automatic measurement system is our goal for this project. Also, based on the experimental results, the measurement of the fourth parameter of the Stokes vector was not precise enough. Finding the reason for this problem and solving it will be another task for future work.

ACKNOWLEDGMENTS

This research was supported in part by the Ministry of Education, Culture, Sports, Science and Technology under the Leading Project, “Development of High Fidelity Digitization Software for Large-Scale and Intangible Cultural Assets.” Daisuke Miyazaki was supported by the Japan Society for the Promotion of Science. The authors thank Joan Knapp for proofreading and editing this manuscript.

REFERENCES

1. D. Miyazaki and K. Ikeuchi, “Inverse Polarization Raytracing: Estimating Surface Shape of Transparent Objects,” in *Proceedings of IEEE Computer Society Conference on Computer Vision and Pattern Recognition*, pp. II:910–917, San Diego, CA USA, June 2005.
2. W. A. Shurcliff, *Polarized light: production and use*, p. 207, Harvard University Press, Cambridge, Mass, 1962.
3. Y. Y. Schechner, J. Shamir, and N. Kiryati, “Polarization and statistical analysis of scenes containing a semireflector,” *Journal of Optical Society of America A*, vol. 17, no. 2, pp. 276–284, 2000.
4. L. B. Wolff and T. E. Boult, “Constraining object features using a polarization reflectance model,” *IEEE Transactions on Pattern Analysis and Machine Intelligence*, vol. 13, no. 7, pp. 635–657, 1991.
5. S. K. Nayar, X.-S. Fang, and T. Boult, “Separation of Reflection Components Using Color and Polarization,” *International Journal of Computer Vision*, vol. 21, no. 3, pp. 163–186, 1997.
6. S. Lin and S. W. Lee, “Detection of Specularity Using Stereo in Color and Polarization Space,” *Computer Vision and Image Understanding*, vol. 65, no. 2, pp. 336–346, Feb. 1997.
7. S. Umeyama and G. Godin, “Separation of Diffuse and Specular Components of Surface Reflection by Use of Polarization and Statistical Analysis of Images,” *IEEE Transactions on Pattern Analysis and Machine Intelligence*, vol. 26, no. 5, May 2004.

*Developing “Polavision” and related algorithms was mainly performed by Noriyuki Takashima, Akira Yoshida, and Eiki Harashima. Developing “Cocoon” and related algorithms was mainly performed by Daisuke Miyazaki and Katsushi Ikeuchi.

8. T. Shibata, T. Takahashi, D. Miyazaki, Y. Sato, and K. Ikeuchi, "Creating Photorealistic Virtual Model with Polarization Based Vision System," in *SPIE Proceedings of Conference on Polarization Science and Remote Sensing II (Part of SPIE's International Symposium on Optics and Photonics 2005)*, San Diego, CA USA, Aug. 2005 to appear.
9. K. Hara, K. Nishino, and K. Ikeuchi, "Light Source Position and Reflectance Estimation from a Single View without the Distant Illumination Assumption," *IEEE Transactions on Pattern Analysis and Machine Intelligence*, vol. 27, no. 4, pp. 493–505, Apr. 2005.
10. P. Debevec, T. Hawkins, C. Tchou, H.-P. Duiker, and W. Sarokin, "Acquiring the Reflectance Field of a Human Face," in *Proceedings of ACM SIGGRAPH 2000*, pp. 145–156, New Orleans, Louisiana USA, July 2000.
11. N. Tsumura, N. Ojima, K. Sato, M. Shiraishi, H. Shimizu, H. Nabeshima, S. Akazaki, K. Hori, and Y. Miyake, "Image-Based Skin Color and Texture Analysis/Synthesis by Extracting Hemoglobin and Melanin Information in the Skin," *ACM Transactions on Graphics (Proceedings of ACM SIGGRAPH 2003)*, vol. 22, no. 3, pp. 770–779, San Diego, California USA, July 2003.
12. Y. Y. Schechner, S. G. Narashimhan, and S. K. Nayar, "Polarization-based vision through haze," *Applied Optics*, vol. 42, no. 3, pp. 511–525, Jan. 2003.
13. Y. Y. Schechner and N. Karpel, "Clear underwater vision," in *Proceedings of IEEE Computer Society Conference on Computer Vision and Pattern Recognition*, pp. 536–543, 2004.
14. Y. Y. Schechner and S. K. Nayar, "Generalized Mosaicing: Polarization Panorama," *IEEE Transactions on Pattern Analysis and Machine Intelligence*, vol. 27, no. 4, pp. 631–636, Apr. 2005.
15. O. G. Cula, K. J. Dana, D. K. Pai, and D. Wang, "Polarization Multiplexing for Bidirectional Imaging," in *Proceedings of IEEE Computer Society Conference on Computer Vision and Pattern Recognition*, pp. II:1116–1123, San Diego, CA USA, June 2005.
16. J. Clark, E. Trucco, and L. B. Wolff, "Using light polarization in laser scanning," *Image and Vision Computing*, vol. 15, no. 2, pp. 107–117, Feb. 1997.
17. A. M. Wallace, B. Liang, E. Trucco, and J. Clark, "Improving Depth Image Acquisition Using Polarized Light," *International Journal of Computer Vision*, vol. 32, no. 2, pp. 87–109, Sep. 1999.
18. L. B. Wolff, "Polarization-based material classification from specular reflection," *IEEE Transactions on Pattern Analysis and Machine Intelligence*, vol. 12, no. 11, pp. 1059–1071, Nov. 1990.
19. H. Chen and L. B. Wolff, "Polarization phase-based method for material classification in computer vision," *International Journal of Computer Vision*, vol. 28, no. 1, pp. 73–83, 1998.
20. O. Sandus, "A review of emission polarization," *Applied Optics*, vol. 4, no. 12, pp. 1634–1642, 1965.
21. F. E. Nicodemus, "Directional reflectance and emissivity of an opaque surface," *Applied Optics*, vol. 4, pp. 767–773, 1965.
22. F. E. Nicodemus, "Reflectance nomenclature and directional reflectance and emissivity," *Applied Optics*, vol. 9, pp. 1474–1475, 1970.
23. D. L. Jordan and G. D. Lewis, "Measurements of the effect of surface roughness on the polarization state of thermally emitted radiation," *Optical Letters*, vol. 19, pp. 692–694, 1994.
24. D. L. Jordan, G. D. Lewis, and E. Jakeman, "Emission polarization of roughened glass and aluminum surfaces," *Applied Optics*, vol. 35, pp. 3583–3590, 1996.
25. L. B. Wolff, A. Lundberg, and R. Tang, "Image understanding from thermal emission polarization," in *Proceedings of IEEE Computer Society Conference on Computer Vision and Pattern Recognition*, pp. 625–631, Santa Barbara, CA USA, June 1998.
26. M. Born and E. Wolf, *Principles of optics*, p. 803, Pergamon Press, London, 1959.
27. E. Hecht, *Optics*, p. 698, Addison-Wesley, Reading, Mass., 2002.
28. LightTools, <http://www.opticalres.com/>.
29. ZEMAX, <http://www.zemax.com/>.
30. OptiCAD, <http://www.opticad.com/>.
31. F. Kagalwala and T. Kanade, "Computational model of image formation process in DIC microscopy," in *Proceedings of SPIE*, vol. 3261, pp. 193–204, San Jose, CA USA, Jan. 1998.
32. K. Koshikawa and Y. Shirai, "A model-based recognition of glossy objects using their polarimetric properties," *Advanced Robotics*, Vol. 2, No. 2, pp. 137–147, 1987.

33. L. B. Wolff and D. J. Kurlander, "Ray tracing with polarization parameters," *IEEE Computer Graphics and Applications*, vol. 10, no. 6, pp. 44–55, 1990.
34. R. A. Chipman, "Mechanics of polarizaition ray tracing," *Optical Engineering*, vol. 34, no. 6, pp. 1636–1645, 1995.
35. C. Gu and P. Yeh, "Extended Jones matrix method. II," *Journal of Optical Society of America A*, vol. 10, no. 5, pp. 966–973, 1993.
36. J. S. Gondek, G. W. Meyer, and J. G. Newman, "Wavelength dependent reflectance functions," in *Proceedings of ACM SIGGRAPH 1994*, pp. 213–220, Orlando, Florida USA, July 1994.
37. D. C. Tannenbaum, P. Tannenbaum, and M. J. Wozny, "Polarization and birefringency considerations in rendering," in *Proceedings of ACM SIGGRAPH 1994*, pp. 221–222, Orlando, Florida USA, July 1994.
38. A. Wilkie, R. F. Tobler, and W. Purgathofer, "Combined rendering of polarization and fluorescence effects," in *Proceedings of Eurographics Workshop on Rendering*, pp. 197–204, London, United Kingdom, June 2001.
39. S. Guy and C. Soler, "Graphics gems revisited: fast and physically-based rendering of gemstones," *ACM Transactions on Graphics (Proceedings of ACM SIGGRAPH 2004)*, vol. 23, no. 3, pp. 231–238, Los Angeles, California USA, Aug. 2004.
40. L. B. Wolff, T. A. Mancini, P. Pouliquen, and A. G. Andreou, "Liquid Crystal Polarization Camera," *IEEE Transactions on Robotics and Automations*, vol. 13, no. 2, pp. 195–203, 1997.
41. H. Fujikake, K. Takizawa, T. Aida, H. Kikuchi, T. Fujii, and M. Kawakita, "Electrically-Controllable Liquid Crystal Polarizing Filter for Eliminating Reflected Light," *Optical Review*, vol. 5, no. 2, pp. 93–98, 1998.
42. C. K. Harnett and H. G. Craighead, "Liquid-crystal micropolarizer array for polarization-difference imaging," *Applied Optics*, vol. 41, no. 7, pp. 1291–1296, 2002.
43. G. H. Haertling, "PLZT Electrooptic Ceramics and Devices," *American Chemical Society*, pp. 265–283, 1981.
44. P. E. Shames, P. C. Sun, and Y. Fainman, "Modeling of scattering and depolarizing electro-optic devices. I. Characterization of lanthanum-modified lead zirconate titanate," *Applied Optics*, vol. 37, no. 17, pp. 3717–3725, June 1998.
45. S. Rahmann, "Inferring 3D Scene Structure from a Single Polarization Image," in *SPIE Proceedings of Conference on Polarization and Color Techniques in Industrial Inspection*, vol. 3826, pp. 22–33, Munich, Germany, June 1999.
46. S. Rahmann, "Polarization images: a geometric interpretation of shape analysis," in *Proceedings of International Conference on Pattern Recognition*, pp. 542–546, Barcelona, Spain, Sep. 2000.
47. S. Rahmann and N. Canterakis, "Reconstruction of specular surfaces using polarization imaging," in *Proceedings of IEEE Computer Society Conference on Computer Vision and Pattern Recognition*, pp. 149–155, Kauai Marriott, Hawaii USA, Dec. 2001.
48. S. Rahmann, "Reconstruction of quadrics from two polarization views," in *Iberian Conference on Pattern Recognition and Image Analysis*, pp. 810–820, Mallorca, Spain, June 2003.
49. O. Drbohlav and R. Šára, "Unambiguous determination of shape from photometric stereo with unknown light sources," in *Proceedings of IEEE International Conference on Computer Vision*, pp. I:581–586, Vancouver, Canada, July 2001.
50. D. Miyazaki, R. T. Tan, K. Hara, and K. Ikeuchi, "Polarization-based inverse rendering from a single view," in *Proceedings of IEEE International Conference on Computer Vision*, pp. 982–987, Nice, France, Oct. 2003.
51. M. Saito, Y. Sato, K. Ikeuchi, and H. Kashiwagi, "Measurement of surface orientations of transparent objects by use of polarization in highlight," *Journal of Optical Society of America A*, vol. 16, no. 9, pp. 2286–2293, 1999.
52. D. Miyazaki, M. Saito, Y. Sato, and K. Ikeuchi, "Determining surface orientations of transparent objects based on polarization degrees in visible and infrared wavelengths," *Journal of Optical Society of America A*, vol. 19, no. 4, pp. 687–694, 2002.
53. D. Miyazaki, M. Kagesawa, and K. Ikeuchi, "Transparent surface modeling from a pair of polarization images," *IEEE Transactions on Pattern Analysis and Machine Intelligence*, vol. 26, no. 1, pp. 73–82, 2004.
54. D. E. Zongker, D. M. Warner, B. Curless, and D. H. Salesin, "Environmental matting and compositing," in *Proceedings of ACM SIGGRAPH 1999*, pp. 205–214, Los Angeles, California USA, Aug. 1999.
55. Y. Chuang, D. E. Zongker, J. Hindorff, B. Curless, D. H. Salesin, and R. Szeliski, "Environment matting extensions: towards higher accuracy and real-time capture," in *Proceedings of ACM SIGGRAPH 2000*, pp. 121–130, New Orleans, Louisiana USA, July 2000.

56. Z. S. Hakura and J. M. Snyder, "Realistic reflections and refractions on graphics hardware with hybrid rendering and layered environment maps," in *Proceedings of Eurographics Workshop on Rendering*, pp. 289–300, London, UK, June 2001.
57. W. Matusik, H. Pfister, R. Ziegler, A. Ngan, and L. McMillan, "Acquisition and rendering of transparent and refractive objects," in *Proceedings of Eurographics Workshop on Rendering*, pp. 267–278, Pisa, Italy, June 2002.
58. Y. Wexler, A. W. Fitzgibbon, and A. Zisserman, "Image-based environment matting," in *Proceedings of Eurographics Workshop on Rendering*, pp. 279–290, Pisa, Italy, June 2002.
59. P. Peers and P. Dutré, "Wavelet environment matting," in *Proceedings of Eurographics Workshop on Rendering*, pp. 157–166, Leuven, Belgium, June 2003.
60. H. Farid and E. H. Adelson, "Separating reflections from images by use of independent component analysis," *Journal of Optical Society of America A*, vol. 16, no. 9, pp. 2136–2145, 1999.
61. Y. Y. Schechner, N. Kiryati, and R. Basri, "Separation of transparent layers using focus," *International Journal of Computer Vision*, vol. 39, no. 1, pp. 25–39, 2000.
62. R. Szeliski, S. Avidan, and P. Anandan, "Layer extraction from multiple images containing reflections and transparency," in *Proceedings of IEEE Computer Society Conference on Computer Vision and Pattern Recognition*, pp. 246–253, Hilton Head, SC USA, June 2000.
63. A. Levin, A. Zomet, and T. Weiss, "Separating reflections from a single image using local features," in *Proceedings of IEEE Computer Society Conference on Computer Vision and Pattern Recognition*, pp. I:306–313, Washington DC, USA, June–July 2004.
64. A. Nikolaev and S. K. Nayar, "Transparent grippers: seeing while grasping," in *Proceedings of Image Understanding Workshop*, pp. 1333–1338, Palm Springs, Feb. 1996.
65. M. Osadchy, D. Jacobs, and R. Ramamoorthi, "Using specularities for recognition," in *Proceedings of IEEE International Conference on Computer Vision*, pp. 1512–1519, Nice, France, Oct. 2003.
66. K. McHenry, J. Ponce, and D. Forsyth, "Finding Glass," in *Proceedings of IEEE Computer Society Conference on Computer Vision and Pattern Recognition*, pp. II:973–979, San Diego, CA USA, June 2005.
67. H. Murase, "Surface shape reconstruction of a nonrigid transparent object using refraction and motion," *IEEE Transactions on Pattern Analysis and Machine Intelligence*, vol. 14, no. 10, pp. 1045–1052, 1992.
68. S. Hata, Y. Saitoh, S. Kumamura, and K. Kaida, "Shape extraction of transparent object using genetic algorithm," in *Proceedings of International Conference on Pattern Recognition*, pp. 684–688, Vienna, Austria, Aug. 1996.
69. K. Ohara, M. Mizukawa, K. Ohba, and K. Taki, "3D modeling of micro transparent object with integrated vision," in *Proceedings of IEEE Conference on Multisensor Fusion and Integration for Intelligent Systems*, pp. 107–112, Tokyo, Japan, July–Aug. 2003.
70. M. Ben-Ezra and S. K. Nayar, "What does motion reveal about transparency?," in *Proceedings of IEEE International Conference on Computer Vision*, pp. 1025–1032, Nice, France, Oct. 2003.
71. K. N. Kutulakos, "Refractive and specular 3D shape by light-path triangulation," in *Proceedings of International Symposium on the CREST Digital Archiving Project*, pp. 86–93, Tokyo, Japan, Mar. 2005.
72. W. H. Press, S. A. Teukolsky, W. T. Vetterling, and B. P. Flannery, *Numerical recipes in C: the art of scientific computing*, p. 994, Cambridge University Press, New York, NY USA, 1992.
73. K. Ikeuchi, "Reconstructing a depth map from intensity maps," in *Proceedings of International Conference on Pattern Recognition*, pp. 736–738, Montreal, Canada, Aug. 1984.
74. B. K. P. Horn, "Height and Gradient from Shading," *International Journal of Computer Vision*, vol. 5, no. 1, pp. 37–75, 1990.
75. H. Sato, S. K. Nayar, and K. Ikeuchi, "Implementation and Evaluation of a Three-Dimensional Photometric Sampler," *CMU-RI-TR*, 1990.
76. S. K. Nayar, "Shape Recovery using Physical Models of Reflection and Interreflection," *A Dissertation*, Carnegie Mellon University, May 1991.
77. T. Kiuchi and K. Ikeuchi, "Roughness and shape of specular lobe surfaces using photometric sampling method," in *Proceedings of IEEE Computer Society Conference on Computer Vision and Pattern Recognition*, pp. 765–766, New York, NY USA, June 1993.
78. P. Debevec, A. Wenger, C. Tchou, A. Gardner, J. Waese, and T. Hawkins, "A Lighting Reproduction Approach to Live-Action Compositing," *ACM Transactions on Graphics (Proceedings of ACM SIGGRAPH 2002)*, vol. 21, no. 3, pp. 547–556, San Antonio, Texas USA, July 2002.